PROCEEDINGS OF SPIE

SPIEDigitalLibrary.org/conference-proceedings-of-spie

Modal analysis of pressure fields on and around turrets with different protrusions

Timothy Bukowski, Matthew Kalensky, Stanislav Gordeyev, Matthew Kemnetz

Timothy J. Bukowski, Matthew Kalensky, Stanislav Gordeyev, Matthew Kemnetz, "Modal analysis of pressure fields on and around turrets with different protrusions," Proc. SPIE 12239, Unconventional Imaging and Adaptive Optics 2022, 122390F (4 October 2022); doi: 10.1117/12.2633429

SPIE.

Event: SPIE Optical Engineering + Applications, 2022, San Diego, California, United States

Modal analysis of pressure fields on and around turrets with different protrusions

Timothy J. Bukowski*[a], Matthew Kalensky[b], Stanislav Gordeyev[a], and Matthew Kemnetz[c]

[a]University of Notre Dame, Notre Dame, Indiana, 46556
[b]Integrated Engagement Systems Department, Naval Surface Warfare Center Dahlgren Division, Dahlgren, Virginia, 22448
[c]U.S. Air Force Research Laboratory, Kirtland Air Force Base, New Mexico, 87117

ABSTRACT

Wind tunnel experiments were conducted to measure the unsteady surface pressure field of a hemisphere-on-cylinder turret in subsonic flow. These measurements were obtained using pressure transducers coupled with fast response pressure sensitive paint. The surface pressure field data resulting from Mach 0.5 flow ($Re_D \approx 2 \times 10^6$) over three different turret protrusion distances were analyzed. Previously, dominant surface pressure modes on the turret were found using proper orthogonal decomposition. The results of which showed that greater turret protrusion into the freestream flow increased the prevalence of spanwise anti-symmetric surface pressure field fluctuations. These anti-symmetric pressure fluctuations are caused by anti-symmetrical vortex shedding. However, when a partially submerged hemispherical turret geometry is used, it was shown that this anti-symmetric mode was of much lower relative energy. This suggests that there is a transition in flow field phenomena as protrusion is changed from partially submerged to a full hemisphere configuration. Further investigation into this so-called "mode switching" is the emphasis of the work presented here. This research heavily relied on modal analysis to identify correlations between turret and wake surface pressure fields. The fluctuations in the surface pressure field around the partial hemisphere were found to be mostly dominated by the wake with little influence from fluidic structures on the turret itself. For the hemisphere and hemisphere-on-cylinder configurations, both symmetric and anti-symmetric unsteady separation grew to be the largest influence and was coupled with the wake fluctuations.

Keywords: Turret, submerged hemisphere, proper orthogonal decomposition, surface pressure, directed energy, hemisphere-on-cylinder, pressure sensitive paint, modal analysis

1. INTRODUCTION

There has been considerable research into integrating directed energy systems into airborne vehicles[1–3]. Hemisphere shaped geometries are of high interest for beam director designs due to their fairly simple geometry and wide field-of-regard. The general behavior for a flow around a hemisphere-on-cylinder has been discussed extensively in Gordeyev et al. [4] and will only be briefly summarized here. As flow stagnates at the front of the turret, a "necklace" vortex forms and extends downstream around the base of the turret, as schematically shown in Fig. 1. This necklace vortex is heavily influenced by the state of the incoming boundary layer. The flow over the front of the turret is relatively steady with a stagnation line forming along the leading edge of the cylinder, and attached flow accelerating over the front portion of the hemisphere. The attached flow eventually separates due to the imposed adverse pressure gradient downstream of the hemisphere's apex. In the separated region, two counter-rotating "horn" vortices form. This turbulent flow field produces unsteady forcing on the turret.

For the application of airborne-mounted laser propagation systems which use turret-based geometries, unsteady forcing of the turret results in vibrations of various optical path components which imposes bulk unsteady angular distortions onto the laser beam [5–7]. Angular beam distortions in the beam director (or at the pupil

*Further author information:
E-mail: tbukowski@nd.edu, Telephone: (574) 631-4280

Unconventional Imaging and Adaptive Optics 2022, edited by Jean J. Dolne, Mark F. Spencer
Proc. of SPIE Vol. 12239, 122390F · © 2022 SPIE · 0277-786X · doi: 10.1117/12.2633429

plane) lead to a net unsteady motion of the laser beam at the target. This rapid far-field beam motion, colloquially referred to as beam jitter, severely reduces the laser power maintained on the desired target aim-point. Jitter resulting from flow-induced vibrations is referred to as aero-mechanical jitter. The unsteady pressure field causing this jitter is only a function of Mach number and turret geometry [8]. Previous studies of the unsteady pressure field around a turret have been performed. Specifically, the effects of different surface features on the unsteady pressure field were studied in [8] and the wake response of an oscillating hemisphere was studied in [9]. Both of these experiments used pressure sensitive paint (PSP) which is able to measure surface pressure fields with very high spatial resolution and has become an increasingly popular method for studying surface pressure fields as its temporal resolution has increased, now being able to measure pressure fluctuations up to 20 kHz [10]. The high spatial resolution PSP provides has made proper orthogonal decomposition of the surface pressure field much more powerful as the relationships between more complex structures in the flow can be visualized.

Hemisphere-on-cylinder turrets with varying protrusions were previously studied in [11], and it was found that there was a significant change in flow behavior from a predominantly symmetric flow to predominantly anti-symmetric flow when transitioning from a partially submerged hemisphere to a full hemisphere. The analysis presented in this paper further studies the same data and the transition from the partial hemisphere to hemisphere geometry. Submerged hemispherical turrets have been studied both experimentally [12,13] and computationally in [14–16]. However, from the results of these studies it is not clear what causes the dramatic change in flow behavior. In this analysis, proper orthogonal decomposition (POD) was used to further understand the prominent structures in the flow over the turret and in the wake. Joint proper orthogonal decomposition (JPOD), introduced in [8], was used to compare flow structures between different geometries.

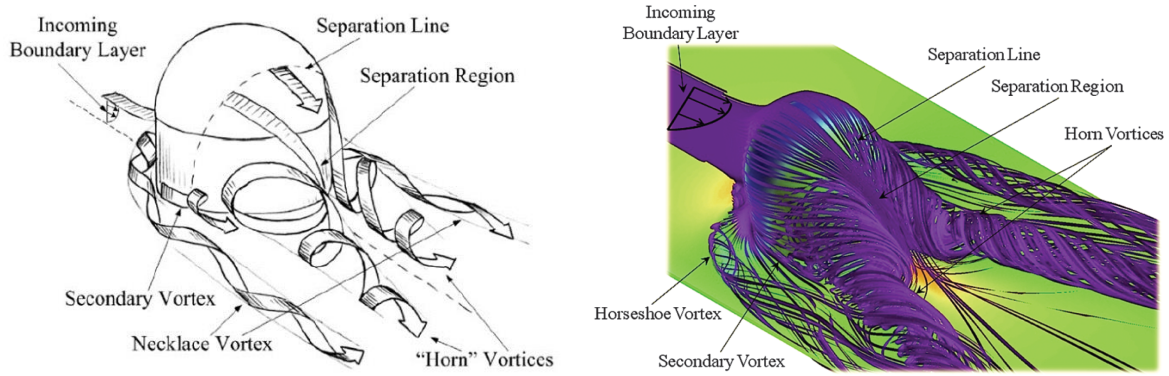

Figure 1. Schematic of major flow structures for flow around a hemisphere-on-cylinder turret[4,15]

2. EXPERIMENTAL SETUP

Surface pressure was measured for flow over a hemisphere-on-cylinder turret with varying protrusion in Mach 0.5 subsonic flow. The setup has already been described in depth in [11], so it will only be summarized here. For these studies, the same turret with diameter D= 0.30 m (12 in) was used. This turret is a shell of the AAOL turret which has produced many foundational datasets and impactful results [17–19] in the aero-optics community. It is worth noting that the AAOL shell turret model used in the studies presented here is not a smooth hemisphere-on-cylinder, but rather has realistic surface features such as small gaps between the stationary turret shell and the rotating "donut" part, screw holes, etc. An image of this turret configured in the wind tunnel can be seen in Fig. 2. The turret protruded from the wall at different heights of $H = 0.07$ m (2.75 in), 0.15 m (6 in), 0.19 m (7.5 in), and 0.27 m (10.5 in). The lowest protrusion is referred to as the "partial hemisphere," which corresponds to about 45% of the hemisphere protruding. The $H = 0.15$ m protrusion configuration is referred to as the "hemisphere" case and the $H = 0.19$ m protrusion configuration is referred to as the "hemisphere + cylinder" case. The $H = 0.27$ m protrusion case was not included in this analysis as it was noisy and did not provide much additional insight. The different geometries were tested in the University of Notre Dame's White Field Mach 0.6 wind tunnel. This wind tunnel has a 0.91 x 0.91 m (3 by 3 ft) test section and data were collected

at freestream Mach numbers of 0.3, 0.4, and 0.5. However, the analyses presented in this paper are focused on protrusion distance effects for only the Mach 0.5 case due to the favorable signal to noise ratio at this Mach number. Initial results and analysis from Mach 0.3, 0.4 as well as the 0.27 m protrusion cases are discussed in [11]. A fast response polymer-ceramic pressure sensitive paint (PC-PSP) was used to measure the surface pressure on the surface of the turret and inside the 0.3 x 0.61 m (12 x 24 in) wake region behind the cylinder, which can be seen in Fig. 2 (Left). The PSP was excited by 8 UV-light sources, visible in Fig. 2 (Left) and the resulting luminescence intensity was measured. Two synchronized high-speed Phantom cameras (v1611 and v2512), one on each side of the test section, were used to capture the PSP intensity with a 3 kHz frame rate. Four Kulite XT-140 pressure transducers were installed into the surface of the turret, as shown in Fig. 2. These wall-mounted fast-response pressure transducers allowed for the in-situ calibration of the PSP. Data collection of the pressure transducers was synchronized with the cameras and recorded unsteady pressures for 5.33 seconds at a sampling rate of 30 kHz. Tunnel temperature, static pressure, and lab atmospheric pressure were recorded before and after tests. More information about the PSP and its application can be found in [20,21].

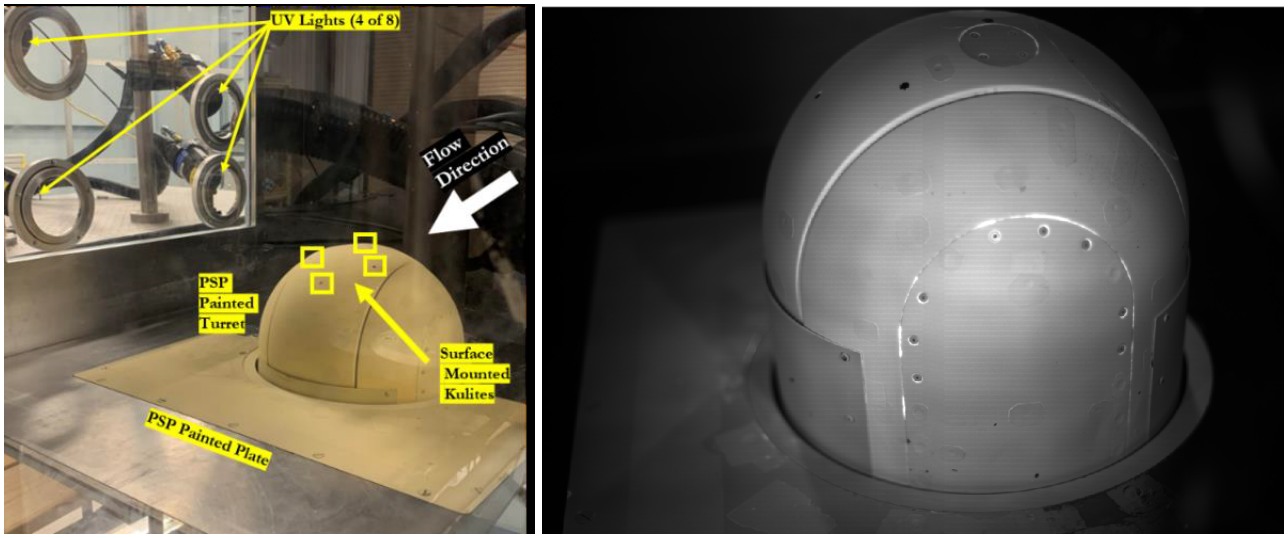

Figure 2. (Left) Turret set-up inside the wind tunnel. Beige regions are where PSP was applied. (Right) Sample image from PSP video for full 10.5 in protruded turret.

3. DATA REDUCTION

3.1 Surface pressure reconstruction

The general process for surface pressure reconstruction and PSP calibration was the same as in [8,11]. However, in these studies, there were changes in the mesh and blending used to extract pressure from the raw imagery data. As before, the 2-D images from the two cameras were transformed into a 3-D surface which allowed for more freedom in viewing the data from different angles and made it possible to combine the two datasets to get a full image of the turret and the wake region. This conversion was done using a perspective transformation matrix (PTM), which is created using an image of a mask with points at known locations in 3-D space. A 3-D mesh was created, then mapped onto the 2-D image plane which is shown in Fig. 3. The mesh in the wake region was rectangular with grid steps of 7.6 mm (0.3 in), while the dome had a spherical mesh with grid steps of 3° in both azimuthal and elevation directions. Mesh points were not included at the locations of the unsteady pressure sensors since the wall-mounted sensors themselves were not painted. For the hemisphere and hemisphere + cylinder cases, small semi-circular regions at the front and the aft portions of the turret, visible in Fig. 4, were also excluded from the turret mesh. The reason for the exclusion is that these regions were seen by the cameras at severely oblique angles (> 80 degrees), and PSP angular response at these large angles is hard to quantify. Finally, mesh points were not included in the region where the turret body meets the tunnel wall as the transition could not be clearly defined in the images.

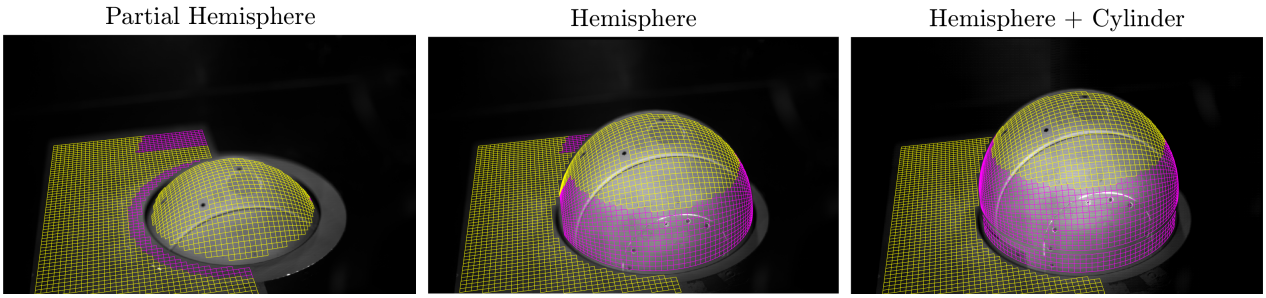

Figure 3. Mesh used to collect data which has been overlayed on top of an example image. The region in yellow is the common region used for JPOD. The purple and yellow regions together were used for POD. Flow goes from right to left.

The intensities for pixels closest to the mesh locations were extracted and spatially filtered by taking the average value of pixels in an 11 x 11 surrounding square. The intensity values, I, recorded by the cameras were converted to static pressure, P, through the Stern-Volmer equation

$$\frac{I_{ref}(s)}{I(s,t)} = A + B\frac{P(s,t)}{P_{ref}} \tag{1}$$

where P_{ref} was the ambient lab pressure and I_{ref} is the temporal mean of the reference data taken with the wind tunnel flow off and the UV lights on. A and B are calibration constants calculated for each camera and geometry using the temporal mean pressure from the unsteady pressure sensors and intensity values from pixels surrounding the pressure sensor. The calibration curves are shown in [11]. Only pressure fluctuations were used in this analysis. However, there was a temperature-related drift in the mean that was found in the PSP data. Since the temperature drift was mostly linear, a linear component was subtracted from the intensity time series to ensure the pressure fluctuations are not affected by the temperature drift.

After conversion to spatial pressure fields, the sets of data from two cameras were combined to get a full surface pressure field. This was accomplished by using weighted blending functions, similar to the method used in [8]. For the dome, a region of 20 mm on either side of the centerplane in the spanwise direction was averaged following a linearly varying weighted average. For the wake region, no weighting was used and all points with values from both cameras were averaged evenly.

3.2 Proper orthogonal decomposition

As in the previous paper [11], Proper Orthogonal Decomposition (POD) was used to analyse the unsteady pressure fields on the turret and in the wake region. POD is commonly used as a means for creating a low-order reconstruction of the spatio-temporal data, where the data can be represented using a reduced number of spatial modes [22]. In POD, the globally-reconstructed spatio-temporal fluctuating pressure field, $p(s,t)$, where $s = (x, y, z)$ denotes a spatial point, is decomposed into a series of spatial POD modes, $\phi_n(s)$, and corresponding temporal coefficients, $a_n(t)$, such as $p(s,t) = \sum_n a_n(t)\phi_n(s)$. The POD modes are the solutions of the eigenvalue problem,

$$\int_{s'} R(s,s')\phi_n(s')ds' = \lambda_n\phi_n(s), \tag{2}$$

where $R(s,s') = \overline{p(s,t)p(s',t)}$ is the two-point cross-correlation martix and the overbar denotes the temporal averaging. The energy of each mode is given by the eigenvalue, λ_n. By construction, the POD modes are orthonormal, $\int_s \phi_n(s)\phi_m(s)ds = \delta_{nm}$, where δ_{nm} is a Kronecker delta. The temporal coefficients can be found by projecting the pressure field onto the POD mode,

$$a_n(t) = \int_s p(s,t)\phi_n(s)ds. \tag{3}$$

The energy of each mode can be also found directly from the temporal coefficients as $\lambda_n = \overline{a_n^2(t)}$.

Equations (2) and (3) were discretized using the mesh explained in the Section 3.1 and combines the purple and yellow meshes in Fig. 3, to decompose the surface pressure PSP data into individual POD modes and their coefficients. Since the mesh was nonuniform, a weighted version of POD calculation was implemented [22, 23]. The MATLAB `eig` function was used to solve Equation (2).

3.3 Joint POD

Although an optimal set of modes can be obtained for each data set using POD, the spatial modes are different for each case, so comparing POD modes and related energies for different turret geometries becomes complicated. An alternative way, called Joint Proper Orthogonal Decomposition (JPOD), was proposed and used as a data analysis technique to compute the common or joint modes from different data sets [8, 9]. JPOD is a specialized version of POD, in which the spatio-temporal data for different cases are combined into a single joint data set, and POD algorithm is used to extract the joint spatial modes. In the present studies, the cross-correlation matrices for all turret configurations were combined to compute a *joint* two-point cross-correlation matrix, $R_{Joint}(s, s')$,

$$R_{Joint}(s, s') = R(s, s'; PartialHemisphere) + R(s, s'; Hemisphere) + R(s, s'; Hemisphere + Cylinder) \quad (4)$$

where the $R(s, s', Geometry)$ is the correlation matrix of a given geometry normalized by the square of the spatial mean of the temporal root mean square of its pressure field, $\langle P_{rms}(s)\rangle^2$, where the angle brackets denote spatial average. The JPOD requires a common surface area and mesh to be defined, which is shown in yellow in Fig. 3. The joint POD modes, $\psi(s)$, were computed, using $R_{Joint}(s, s')$ via Equation (2). The temporal coefficients of JPOD modes, denoted as $b(t; Geometry)$, were computed by projecting the JPOD modes onto *individual* pressure fields,

$$b_n(t; Geometry) = \int_s p(s, t; Geometry)\psi_n(s)ds. \quad (5)$$

From the temporal coefficients, individual energies of JPOD modes were computed,

$$\Lambda_n(Geometry) = \overline{b_n^2(t; Geometry)}. \quad (6)$$

By design, this set of spatial JPOD modes is the same for all cases. When the individual data sets for each case are projected onto these spatial JPOD modes, only the temporal coefficients and the corresponding energies will be different. Thus, the differences among cases will be reflected only in the temporal coefficients and the energy distributions, making it easier to compare the cases.

4. RESULTS

4.1 Pressure fields

The PSP data were used to calculate the surface pressure fields for each of the different turret geometries. Subsequently, the spatial map of the pressure fluctuation coefficient, $C_{p,rms}(s)$, was calculated, and the results are shown in Fig. 4. Similar calculations were presented in [11]; however, the results presented here were calculated with a mesh that was extended to the wake region to provide a more complete view of the pressure field around the turrets. The quarter circle visible in the bottom left ∼(Z=-0.15, X=0.2) of the plots is a consequence of the mesh and blending, and is not a physical feature of the flow. The separation line is clearly visible for the hemisphere and hemisphere + cylinder, however, the flow is separating just behind the apex of the turret. This separation location is sufficiently further upstream than expected. Flow over a hemisphere and hemisphere + cylinder is expected to separate at approximately 120° from the freestream direction (measured from -X axis) for flows with $Re_D > 300,000$ [4], where this presented flow is around $Re_D = 2 \times 10^6$. This early separation is likely caused by imperfections on the surface of the turret. The separation line location is similar to that observed in previous experiments using the same turret with these realistic surface features in [8]. The spanwise extent of the wake is the smallest for the partial hemisphere and becomes wider for the hemisphere and the hemisphere + cylinder cases. Also, pressure fluctuations on the turret surface and in the wake region increase with the amount of protrusion, with the smallest fluctuations observed for the partial hemisphere case and the largest fluctuations for the hemisphere + cylinder case.

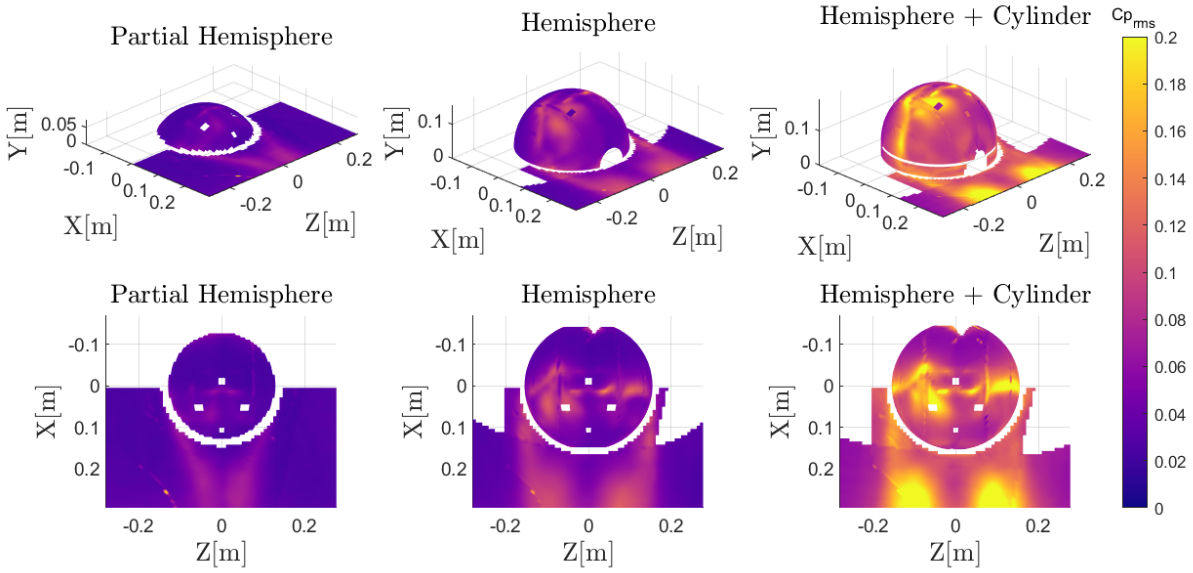

Figure 4. Spatial maps of pressure fluctuation coefficients, $C_{p,rms}(s)$, for each geometry. Flow goes in positive X direction.

4.2 POD Analysis

Proper orthogonal decomposition (POD) was performed on the fluctuating pressure fields to study prominent spatial features in the flow. POD was performed for the wake and dome regions together which are shown in Fig. 3 as the purple and yellow meshes. This allowed us to relate flow features from the two regions. The first four POD modes for each geometry are shown in Fig. 5 along with the modes' associated relative energy. The relative energies of the first ten modes for the three geometries are show in Fig. 6.

The hemisphere and hemisphere + cylinder geometries have almost identical modes, except the hemisphere + cylinder has higher energy. The first mode contains 16% and 21% of the total energy for the hemisphere and hemisphere + cylinder, respectively. This mode is mostly anti-symmetric in the cross-stream direction. The pressure fluctuations from the separation line are correlated with the separated region of the wake. This correlation is shown in Fig. 5 where areas with dark blue are strongly correlated, and yellow regions are anti-correlated with the dark blue region, with green begin neutral. The anti-symmetric nature of mode 1 is a result of unsteady alternating vortex shedding that has been seen throughout literature [4,8,24]. The second mode for the hemisphere and hemisphere + cylinder geometries, which contains 10% and 11% of the total energy, respectively, looks similar to the $C_{p,rms}(s)$ maps with the strong correlation on the top of the sphere corresponding to the fluctuations from the separation region. This region is rather thick and not uniform in the cross-stream direction due to the surface features on the top of the hemisphere some of which appear in the POD mode. Also evident is a pair of correlated regions in the wake related to the counter-rotating horn vortices. The flow moving over the top of the turret is pulled downward towards the wall which is visualized nicely in Fig. 1 (Right). At the point where this downwashed flow reattaches to the wall, there is a relatively large increase in pressure. For mode 2 this wake reattachment region and the separation region are anti-correlated, which is similar to what [25] described as a wake "breathing" mode. As the separation line moves upstream it causes an increase in pressure on top of the turret, as it is now in the separated region, while at the same time causing a decrease in pressure at the wake reattachment location. The decrease could be because the flow, which separates earlier than the apex, is moving slower so it has less momentum to hit the wall with at reattachment. Then if the separation line moves downstream we get opposite effects. From modes 1 and 2, we see that the separation line on the turret is fairly strongly correlated to the wake structures. It is interesting to note that these two modes contain different wake structures and since POD modes are statistically uncorrelated, the separation zone in mode 1 and the wake reattachment zone in mode 2 were statistically uncorrelated. However, they do both appear in mode

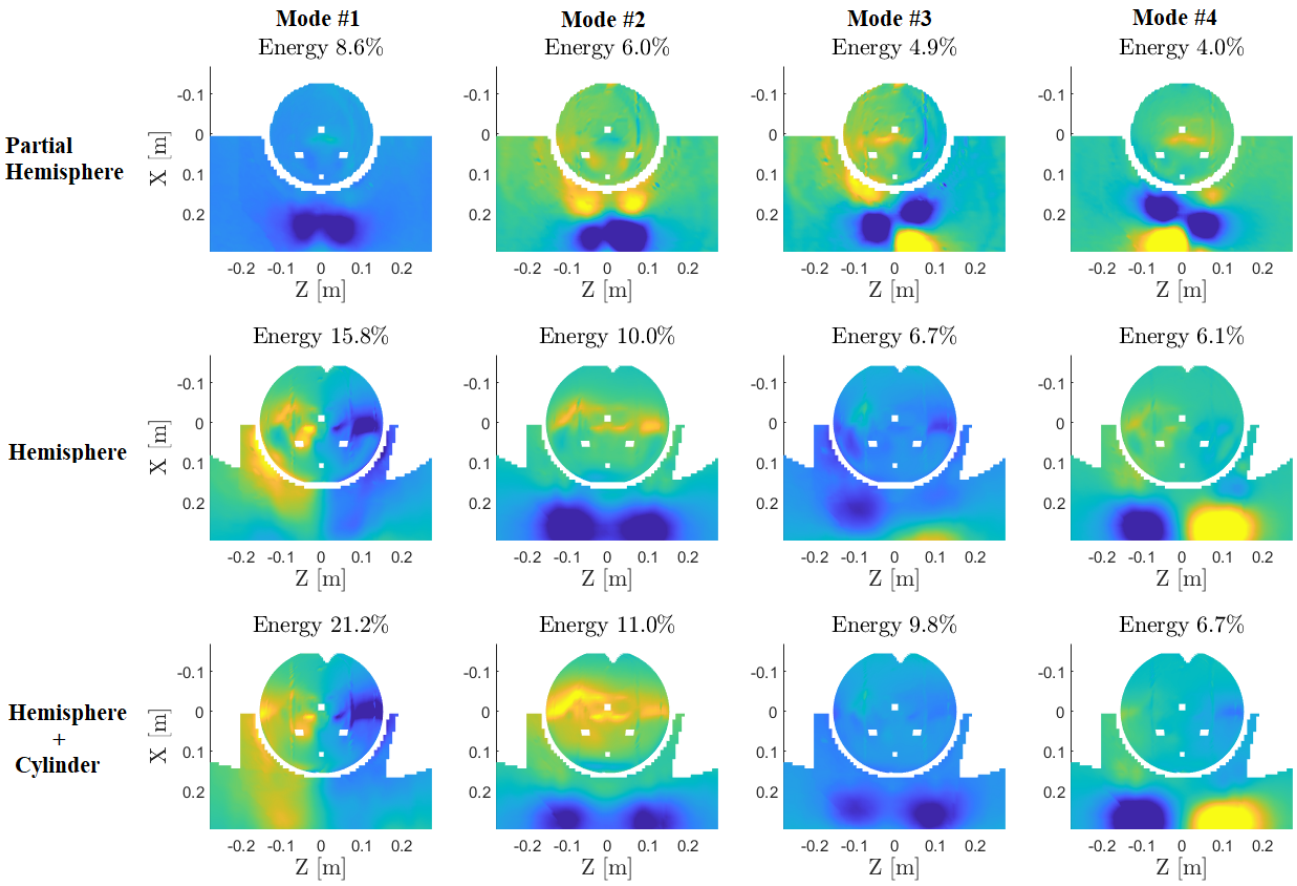

Figure 5. POD modes for each geometry with associated modal energy.

4 so they are not completely independent. The third mode for the two geometries show correlation of the wake but there is very little correlation with anything on the turret, aside from some regions of the separation line for the hemisphere, which shows a decoupling of the wake from the turrets geometry for this mode. Also for the hemisphere mode 3, there is a slight asymmetry. Mode 4 shows a strong anti-correlation in the wake similar to mode 1, which is again related to the alternating vortex shedding off of the turret. This mode was also seen in [26] where the alternating pockets continued downstream, which in this case, if the wake region was extended downstream, we would expect to see another set of correlated regions, but with a blue region on the positive Z side and a yellow region on the negative Z side. This mode also has anti-correlation between the dome and the wake as was seen in mode 2. Here, there is also a slight correlation between the flow on the top of the dome, and the flow wrapping around the base of the turret, similar to mode 1.

Fundamentally different behavior is noticed in the POD modes for the partial hemisphere geometry compared to the hemisphere and hemisphere + cylinder geometries. The primary mode, containing 8% of the total modal energy, is symmetric with two pockets of highly correlated fluctuation in the wake corresponding to the reattachment explained previously. As there is very little correlation with any region on the turret, aside from a weak correlation with the short separation line on top of the turret, the wake for the partial hemisphere is mostly decoupled from the turret, which is a prominent departure from the flow dynamics over the hemisphere and hemisphere + cylinder which had strong correlation between the separation line and the wake for the first two modes. The second mode containing 6% of the energy is also related to the vortices in the wake and is also symmetric. However, there is now a region of anti-correlated fluctuation shown in yellow in between the turret and the further downstream wake structure shown in blue. There is a faint blue region on the top of the dome around (0,0), with a faint yellow region on the downstream section of the dome. This mode could be thought

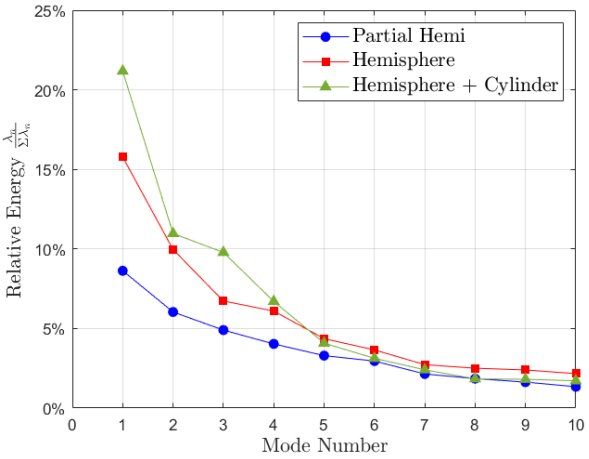

Figure 6. POD modal energy for each geometry.

of as a companion mode to the first mode showing movement of the reattachment region up and downstream. As the high pressure reattachment region moves upstream, the region upstream would see a pressure increase, while the region downstream which no longer has flow reattaching over it would experience a decrease in pressure. In this case, the yellow region of the mode would correspond to the region of increasing pressure while the blue region would correspond to the decreasing pressure region. If the reattachment region instead moves downstream, the direction of change in pressure would flip with the yellow corresponding to dropping pressure and the blue corresponding to increasing pressure. Another possible interpretation of this mode would be that the yellow region corresponds to the fluctuation of the reattachment lines along the sides of the separated region, while the blue region is the same as the blue region in mode 1. Modes 3 and 4 are again related to the structures in the wake, but also include contribution from flow over the top of the dome. They are slightly asymmetric both in the wake and on the dome, but not as anti-symmetric between positive and negative Z as seen in mode 4 for the other geometries. The asymmetries are slightly offset which may be explained by a much less dramatic alternation in the vortices shedding mostly from the top instead of around the sides of the turret. This mode seems to be approaching the alternating vortices seen in mode 4 for the hemisphere and hemisphere + cylinder. These modes all look fairly similar and from all of them together, we can see the vortex structures fluctuating and shedding downstream. From these modes we can also see that the wake is getting larger as protrusion increases, based on the size of the dark blue region in mode 1 for the partial hemisphere and mode 2 for the hemisphere and hemisphere + cylinder. In the plot of modal energies of the different geometries in Fig. 6 we can see that the flow grows more "organized" as protrusion increases as the leading modes contain more of the total energy of the system. The first three modes for the hemisphere and hemisphere + cylinder contain 32% and 42% of the total energy respectively, whereas for the partial hemisphere the first three modes only contain 20% of the total energy.

To understand the temporal dynamics of the these dominant structures in the pressure field, spectra of the time coefficients for the first four modes of each geometry were calculated. The spectra were calculated using a Hanning window and block averaged using 10 blocks. The results which can be seen in Fig. 7 are plotted against Strouhal number, $St_D = fD/U_\infty$, which is then normalized frequency based on the turret diameter.

For the hemisphere, spectra are shown in the top right plot of Fig. 7. The anti-symmetric Modes 1 and 4 have noticeable peaks at $St_D \approx 0.18$. This is consistent with results obtained in [8,26] and is associated with anti-symmetric vortex shedding. The spectra of modes 2 and 3 for the hemisphere do not have any noticeable peaks. The hemisphere + cylinder case shown in the bottom plot of Fig. 7 does not have a distinct peak for the first mode, but rather has high energy for all low frequencies up to $St_D \approx 0.2$, above which it drops off. For mode 4 there is a clear peak at $St_D \approx 0.2$. As with the hemisphere, modes 2 and 3 do not have any prominent peaks. For the partial hemisphere the first mode has high energy in the lower frequencies with a peak at $St_D \approx 0.27$,

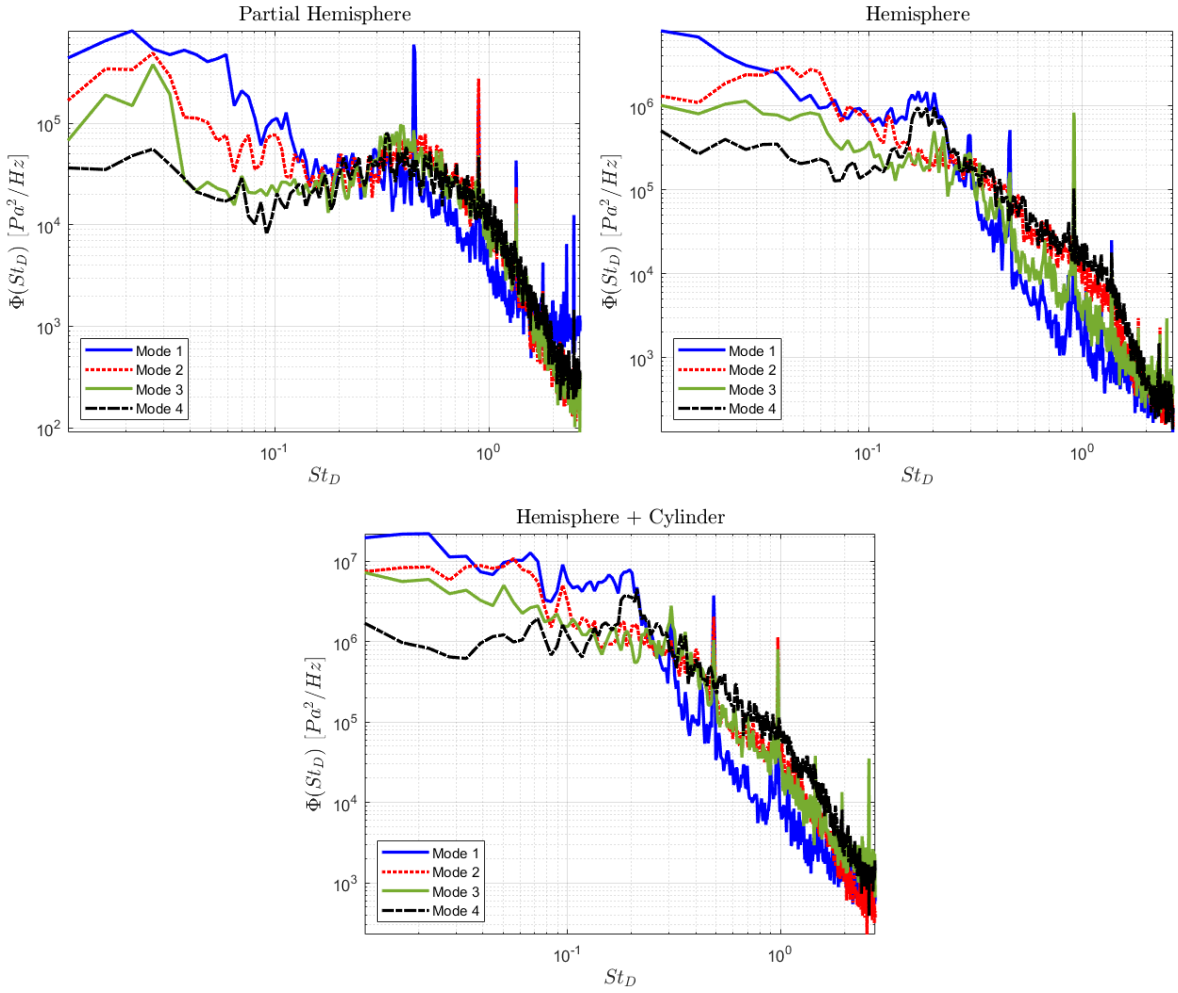

Figure 7. Spectra of time coefficients for POD modes 1-4 for each geometry.

while modes 2-3 have a clear hump that peaks around $St_D \approx 0.45$. These peak fall in the range of $St_D = 0.2-0.5$ that is associated with symmetric vortex shedding [24]. There are also sharp peaks throughout the spectra that are likely from the equipment electronic noise. In addition to having a peak at a different location compared to the hemisphere and hemisphere + cylinder spectra, the partial hemisphere has a much different spectra shape with a much more gradual hump. For all modes and turret geometries, the lower frequencies $St_D < 0.5$ contain most of the spectral energy. It is worth noting that the partial hemisphere modes 3 and 4 have a higher peak frequency than mode 4 for the hemisphere and hemisphere + cylinder, as these modes seem similar. As suggested before, it seems like the partial hemisphere modes 3-4 would turn into hemisphere mode 4 as the protrusion is increased, and based on the spectral peaks, we can see the frequency would decrease as well. A possible source of this change could be the separation occurring on the turret, which seems to increase greatly in strength and correlation with the wake between the partial hemisphere and hemisphere, based on its presence in the first two modes. Also, it is a bit unusual how the correlation is not very strong for the separation line in any of the modes for the partial hemisphere, suggesting weak separation dynamics. These results also somewhat disagree with previous numerical studies where separation over a partial hemisphere was clearly evident [14,15], so additional studies are needed to resolve this issue. In the partial hemisphere mode 3, the unsteady separation line is a little clearer extending from about Z=0.05 all the way to the edge of the turret at about Z=-0.1.

4.3 Joint POD Analysis

While we can gain good insight into the effects of different protrusions through POD, JPOD allows for a much more direct comparison of the prominent flow features between different geometries. The pressure fluctuation data was used to perform JPOD analysis. The first five modes are shown in Fig. 8. These modes are almost identical to the regular POD modes of the hemisphere and hemisphere + cylinder and follow the same interpretation. Mode 5 for the POD was not shown, however, for the hemisphere and hemisphere + cylinder it was also similar to the JPOD mode 5. This mode has a pair of correlated structures in the wake colored yellow that are anti-correlated with another pair of structures downstream which are shown in blue, and also anti-correlated to the separation line region on top of the dome, also blue. This mode is similar the the POD mode 2 for the partial hemisphere and is related to the wake "breathing." As explained for the partial hemisphere mode 2, this JPOD mode 5 can be thought of as a companion mode to JPOD mode 4, corresponding to the up and downstream movement of the reattachment point.

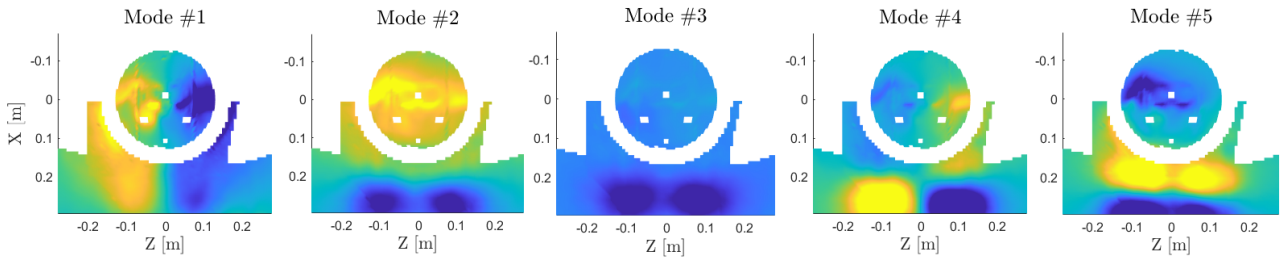

Figure 8. JPOD modes.

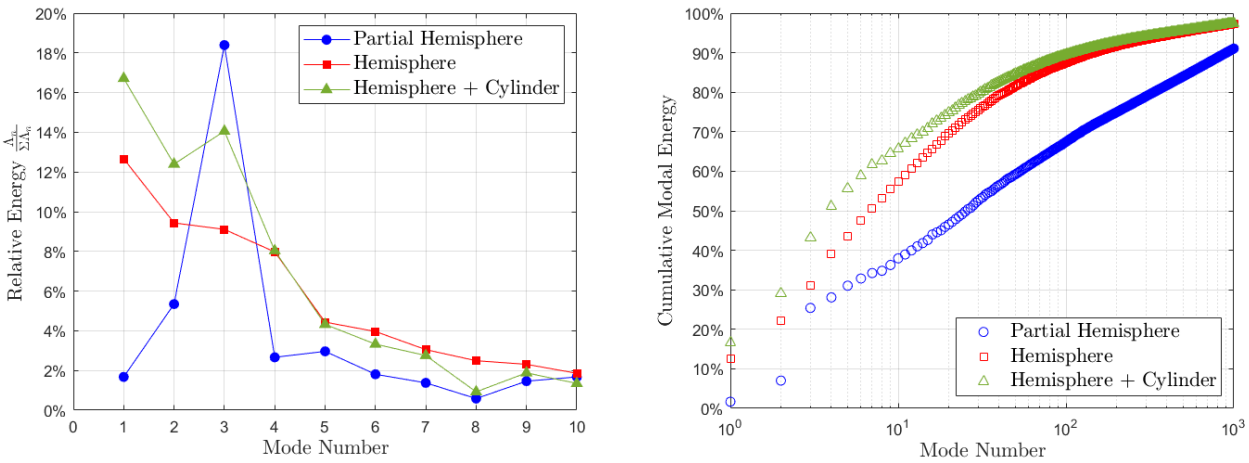

Figure 9. JPOD mode energy and cumulative energy for each geometry.

In the plot of energy shown in Fig. 9 the shift in dominant modes between the partial hemisphere and hemisphere is obvious. The primary mode for the partial hemisphere is mode 3, with 19% of the total energy, which is a symmetric mode related to the wake, where the most energetic mode for the hemisphere and hemisphere + cylinder is mode 1, with 13% and 17% of the total energy, respectively, which is an anti-symmetric mode related to the separation off the sides of the turret and the separated region. Mode 2 is the second most energetic mode for the hemisphere with 10% of the total energy and is the third most energetic for the hemisphere + cylinder containing 13%. For the partial hemisphere, this mode has a lower relative energy of 6%. Interestingly, however, this mode is still the second most energetic for the partial hemisphere; showing there is in fact some inverse

relation between the flow on top of the turret and the wake for the partial hemisphere, despite not showing up clearly in the POD modes

Mode 3 is prominent for all three geometries being the most energetic mode for the partial hemisphere (18%), the second energetic mode for the hemisphere + cylinder with 14% of the energy, and the third energetic mode for the hemisphere with 10%. This leads us to conclude that a coherent wake is a significant flow feature for all geometries. As for mode 1, while it is the primary mode for the hemisphere and hemisphere + cylinder, it is not even in the top 5 modes for the partial hemisphere case with less than 2% of the total energy. Therefore, between the 45% protrusion of the partial hemisphere and the full hemisphere protrusion, the anti-symmetric separation and "horn" vortices grow more prominent. With the increased protrusion, the separation in general becomes stronger, and mode 2 also increases in relative strength. It doesn't appear as though mode 3 loses energy as protrusion increases, since this mode has relatively high energy for all geometries. Mode 4 seems like a combination of modes 1 and 2, with anti-correlation side to side and dome to wake. Mode 5 is similar to mode 2 with anti-correlation between the separation line and the wake, however, there is an additional anti-correlated wake region. This mode is the the 3rd highest energy mode for the partial hemisphere, and it is similar to the partial hemisphere's POD mode 2. However, despite being the third mode, it only holds a relatively low 3% of the total energy. For the hemisphere and hemisphere + cylinder, this mode is the fifth most energetic, however, it holds a higher portion of energy than the partial hemisphere at 5% of the total energy.

From the cumulative energy plot in Fig. 9 we can get an idea of the organization of flow for the different geometries. As protrusion decreases, the cumulative energy decrease consistent with the smaller Cp_{rms} values observed in Fig. 4. The hemisphere + cylinder is most organized requiring about 110 modes to have 90% of the total energy, while the hemisphere requires about 150 modes, and the partial hemisphere, which is significantly less organized, requires about 900 modes to reach 90% of the total energy.

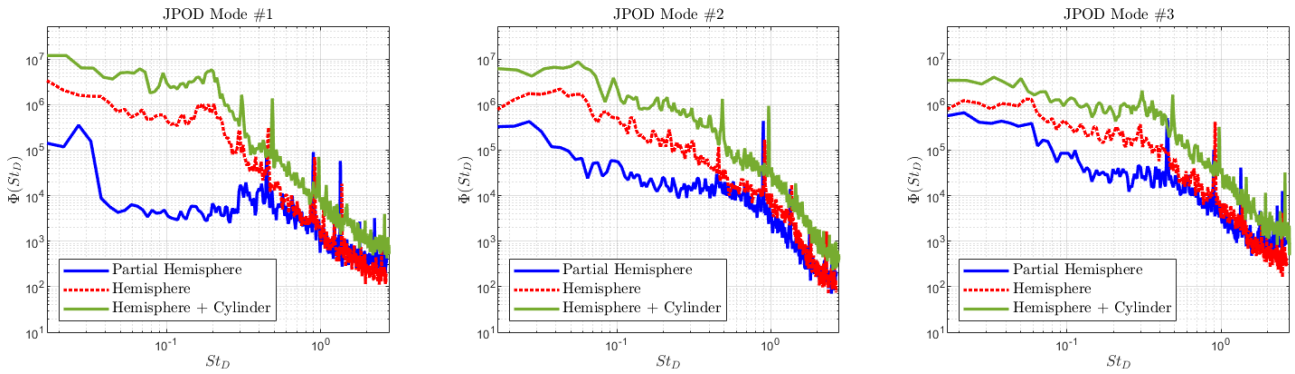

Figure 10. JPOD Spectra.

Spectra of the time coefficients for the first four JPOD modes of each geometry were calculated using a Hanning window and block averaging with 16 blocks that are 0.33 seconds in length. The spectra of the first three modes are plotted versus Strouhal number, St_D, in Fig. 10. For mode 1 corresponding to the asymmetric correlation, the spectra of the hemisphere and hemisphere + cylinder look similar to the spectra of their POD mode 1 which is expected as the JPOD and POD mode 1 look very similar. Both have a peak at $St_D \approx 0.19$, which again is associated with the asymmetric vortex shedding. The hemisphere + cylinder case has a clearer peak with less energy in the lower frequencies below $St_D \approx 0.19$ than the spectra of its POD mode 1. The partial hemisphere has much lower energy in the lower frequencies than the other two geometries, with a peak at $St_D \approx 0.4$. The energy for frequencies higher than this drops off, following the spectra of the hemisphere fairly closely. For mode 2 corresponding to the separation-wake relationship, the hemisphere and hemisphere + cylinder both have higher energy for the lower frequencies that decreases for higher frequencies with no prominent peaks. The partial hemisphere, however, has lower energy for the lower frequencies and has a slight peak around $St_D \approx 0.45$, then dropping off for higher frequencies, again following closely the spectra of the hemisphere. For mode 3, which corresponds to the strong correlation in the wake, the hemisphere and hemisphere + cylinder

have higher spectral energy at lower frequencies, with a slight peak at $St_D \approx 0.3$, and dropping off for higher frequencies. This falls within the range of Strouhal numbers, $St_D \approx 0.2 - 0.5$, expected for symmetric vortex shedding.[24] The partial hemisphere again has lower energy compared to the other two geometries in the higher frequencies with a peak around $St_D \approx 0.45$, then drops off, following the hemisphere spectra.

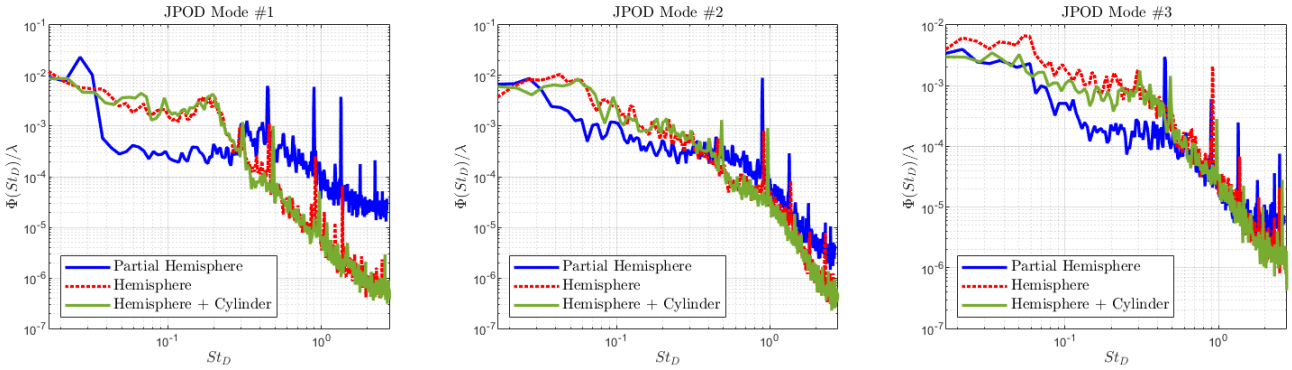

Figure 11. JPOD Spectra Normalized by modal energy.

The spectra were normalized by the energy for a given mode, λ_n, to better compare the relative distribution of energy for the different geometries, which is shown in Fig. 11. The hemisphere and hemisphere + cylinder collapsed very well for modes 1-3. The spectra of the partial hemisphere, however, has a much different shape and doesn't collapse as well. For mode 3 it remains well aligned with the hemisphere, and now the hemisphere + cylinder as well, for higher frequencies. For frequencies between $St_D = 0.06 - 0.4$ the partial cylinder has lower energy than the hemisphere and hemisphere + cylinder. This overall agreement for the three geometries is expected as mode 3 is significant for all three geometries. It also makes sense that there is a drop in energy for the lower frequencies, as these are generally more associated with asymmetric vortex shedding, where the symmetric vortex shedding tends to occur at higher frequencies.[24] For the partial hemisphere, mode 2 has lower energy for the lower frequencies $St_D < 0.4$ and higher energy for the higher frequencies $St_D > 0.4$. For the partial hemisphere, the spectral peak in mode 1 is at a higher frequency than the other geometry's peaks, with its lower frequencies having lower energy and its higher frequencies having higher energy. Overall, the energy of this mode is distributed more evenly across different frequencies than it is for the other geometries.

Normalizing by modes' energies helps to collapse the hemisphere and hemisphere + cylinder cases quite well since their spectra have similar shapes. However, the partial hemisphere has a very different shape so dividing by mode energy just offsets it upward. From Fig. 10, we can see how the partial hemisphere and hemisphere align very well for the higher frequencies. It seems that as the protrusion increases, only the lower frequency energies of these modes increase, up until the full hemisphere is reached. At this point, the energy at all frequencies increases as the cylinder brings the hemisphere away from the wall and more flow is organized into these modes.

5. CONCLUSIONS

In the presented work, surface pressure field measurements were collected over a turret and its wake in order to study the change from a predominantly spanwise symmetric to anti-symmetric flow field as the turret protrusion is increased from a partial hemisphere to a full hemisphere. Pressure sensitive paint was used to measure the surface pressure field for a 0.3 m diameter hemisphere + cylinder turret in Mach 0.5 flow with a Reynolds number of $Re_D \approx 2 \times 10^6$. The protrusions of the turret were varied from 0.07, 0.15 0.19 meters. POD and JPOD modal analyses were performed for the three geometries to investigate the spatial distribution and spectra of different modes. It was found that the surface pressure field of the partial hemisphere was overall less organized compared to the other configurations and no modes were especially dominant. The organization that was present in the modes mostly resulted from the flow in the wake, without much influence from the flow over the turret. However, when the protrusion increases to the hemisphere and hemisphere + cylinder, the unsteady separation becomes much more prominent and is connected to both the separated region and the reattachment region of

the wake. One separation-related mode was a previously proposed spanwise symmetric "breathing" mode.[25] Another significant mode is a strong anti-symmetric vortex shedding mode that becomes the main source of fluctuations in the pressure field and is related to the anti-symmetric fluctuation of the separation line. This anti-symmetric mode has a peak in its spectra at $St_D \approx 0.19$ for the hemisphere and hemisphere + cylinder, where the spectra of these modes had significant decrease in energy at lower frequencies below about $St_D = 0.2$ for the partial hemisphere. It is unclear whether the unsteady separation and anti-symmetric shedding gradually grow with protrusion or whether there is some point which the flow dynamics change suddenly. Overall, POD and JPOD analyses gave similar modes and spectra peaks; however, correlation in the flow related to the unsteady separation line was not as clear in the POD modes for the partial hemisphere. JPOD also provided a more direct comparison between geometries.

ACKNOWLEDGMENTS

This work is supported by the Air Force Research Lab, Cooperative agreement number FA9451-17-2-0088. The U.S. Government is authorized to reproduce and distribute reprints for governmental purposes notwithstanding any copyright notation thereon.

DISCLOSURES

Approved for public release; distribution is unlimited. Public Affairs release approval # AFRL-2022-2804

REFERENCES

[1] De Lucca, N., Gordeyev, S., and Jumper, E., [*The Study of Aero-Optical and Mechanical Jitter for Flat Window Turrets*] (2018).

[2] Kyrazis, D. T., "Airborne Laser Laboratory departure from Kirtland Air Force Base and a brief history of aero-optics," *Optical Engineering* **52**(7), 1 – 6 (2012).

[3] Ross, C. L., "Origins of the airborne laser," *Air Power History* **58**(1) (2011).

[4] Gordeyev, S. and Jumper, E., "Fluid dynamics and aero-optics of turrets," *Progress in Aerospace Sciences* **46**(8), 388–400 (2010).

[5] Kalensky, M., Jumper, E. J., Kemnetz, M. R., and Gordeyev, S., "In-flight measurement of atmospheric-imposed tilt: experimental results and analysis," *Applied Optics* **61**, 4874 (may 2022).

[6] Kalensky, M., *Airborne Measurement of Atmospheric-Induced Beam Jitter*, PhD thesis, University of Notre Dame (2022).

[7] Kalensky, M., Catron, B., Gordeyev, S. V., Jumper, E. J., and Kemnetz, M., "Investigation of aero-mechanical jitter on a hemispherical turret," in [*Proceedings of SPIE*], Dolne, J. J. and Spencer, M. F., eds., SPIE (aug 2021).

[8] Gordeyev, S., De Lucca, N., Jumper, E., Hird, K., Juliano, T., Gregory, J., Thordahl, J., and Wittich, D., "Comparison of unsteady pressure fields on turrets with different surface features using pressure-sensitive paint," *Experiments in Fluids* **55**(1) (2014).

[9] Roeder, A. L. and Gordeyev, S., "Wake response downstream of a spanwise-oscillating hemispherical turret," *Journal of Fluids and Structures* **109**, 103470 (2022).

[10] Gregory, J. W., Asai, K., Kameda, M., Liu, T., and Sullivan, J. P., "A review of pressure-sensitive paint for high-speed and unsteady aerodynamics," *Proceedings of the Institution of Mechanical Engineers, Part G: Journal of Aerospace Engineering* **222**(2), 249–290 (2008).

[11] Kalensky, M., Catron, B., Gordeyev, S., Jumper, E. J., and Kemnetz, M., "Pressure sensitive paint measurements on a hemispherical turret," in [*Unconventional Imaging and Adaptive Optics 2021*], Dolne, J. J. and Spencer, M. F., eds., **11836**, 37 – 53, International Society for Optics and Photonics, SPIE (2021).

[12] Palaviccini, M., Cattafesta, L., and George, B., [*Passive Flow Control over a Three-Dimensional Turret with a Flat Aperture*] (2011).

[13] Woszidlo, R., Taubert, L., and Wygnanski, I., "Manipulating the flow over spherical protuberance in a turbulent boundary layer," *AIAA Journal* **47**(2), 437–450 (2009).

[14] Coirier, W. J., Whiteley, M., Goorskey, D. J., Drye, R., Barber, J., Stutts, J., and Porter, C., [*Aero-Optical Evaluation of Notional Turrets in Subsonic, Transonic and Supersonic Regimes*] (2014).

[15] Jelic, R., Sherer, S., and Greendyke, R., "Simulation of various turrets at subsonic and transonic flight conditions using overflow," *Journal of Aircraft* **50**(2), 398–409 (2013).

[16] Morgan, P. and Visbal, M., [*Effectiveness of Flow Control Over a Submerged Hemispherical Flat-Window Turret*] (2013).

[17] Lucca, N. G. D., Gordeyev, S. V., and Jumper, E. J., "In-flight aero-optics of turrets," *Optical Engineering* **52**(7), 1 – 14 (2013).

[18] Jumper, E. J., Zenk, M. A., Gordeyev, S. V., Cavalieri, D. A., and Whitely, M., "Airborne Aero-Optics Laboratory," *Optical Engineering* **52**(7), 1 – 12 (2013).

[19] Lucca, N. G. D., Gordeyev, S., Morrida, J. J., and Jumper, E. J., [*Investigation of Flow Dynamics Over Turrets with Different Spanwise Aspect Ratios Using PSP*] (2018).

[20] Sakaue, H., Kakisako, T., and Ishikawa, H., "Characterization and optimization of polymer-ceramic pressure-sensitive paint by controlling polymer content," *Sensors* **11**(7), 6967–6977 (2011).

[21] Hayashi, T. and Sakaue, H., "Temperature effects on polymer-ceramic pressure-sensitive paint as a luminescent pressure sensor," *Aerospace* **7**(6) (2020).

[22] Taira, K., Brunton, S. L., Dawson, S. T. M., Rowley, C. W., Colonius, T., McKeon, B. J., Schmidt, O. T., Gordeyev, S., Theofilis, V., and Ukeiley, L. S., "Modal analysis of fluid flows: An overview," *AIAA Journal* **55**(12), 4013–4041 (2017).

[23] Gordeyev, S. and Thomas, F. O., "Coherent structure in the turbulent planar jet. part 1. extraction of proper orthogonal decomposition eigenmodes and their self-similarity," *Journal of Fluid Mechanics* **414**, 145–194 (2000).

[24] Manhart, M., "Vortex shedding from a hemisphere in a turbulent boundary layer," *Theoretical and Computational Fluid Dynamics* **12**(1), 1–28 (1998).

[25] De Lucca, N., *Studies of the pressure field and related beam jitter for hemisphere-on-cylinder turrets*, PhD thesis, University of Notre Dame (2016).

[26] De Lucca, N. G., Gordeyev, S., Morrida, J. J., Jumper, E. J., and Wittich, D. J., [*Modal Analysis of the Surface Pressure Field Around a Hemispherical Turret using Pressure Sensitive Paint*] (2018).